Molecular Biology of the Cell
Vol. 16, 2670–2680, June 2005

Myosin Va Transports Dense Core Secretory Vesicles in Pancreatic MIN6 β-Cells[V]

Aniko Varadi,*† Takashi Tsuboi,* and Guy A. Rutter*

*Henry Wellcome Laboratories for Integrated Cell Signalling and Department of Biochemistry, School of Medical Sciences, University of Bristol, Bristol BS8 1TD, United Kingdom; and †Genomics Research Institute, Centre for Research in Biomedicine, University of the West of England, Bristol BS16 1QY, United Kingdom

Submitted November 16, 2004; Revised February 7, 2005; Accepted March 14, 2005
Monitoring Editor: Benjamin Glick

The role of unconventional myosins in neuroendocrine cells is not fully understood, with involvement suggested in the movement of both secretory vesicles and mitochondria. Here, we demonstrate colocalization of myosin Va (MyoVa) with insulin in pancreatic β-cells and show that MyoVa copurifies with insulin in density gradients and with the vesicle marker phogrin-enhanced green fluorescent protein upon fluorescence-activated sorting of vesicles. By contrast, MyoVa immunoreactivity was poorly colocalized with mitochondrial or other markers. Demonstrating an important role for MyoVa in the recruitment of secretory vesicles to the cell surface, a reduction of MyoVa protein levels achieved by RNA interference caused a significant decrease in glucose- or depolarization-stimulated insulin secretion. Similarly, expression of the dominant-negative–acting globular tail domain of MyoVa decreased by ~50% the number of vesicles docked at the plasma membrane and by 87% the number of depolarization-stimulated exocytotic events detected by total internal reflection fluorescence microscopy. We conclude that MyoVa-driven movements of vesicles along the cortical actin network are essential for the terminal stages of regulated exocytosis in β-cells.

INTRODUCTION

Glucose and other stimuli cause large dense core insulin-containing vesicles (LDCVs) to move toward, and eventually fuse reversibly with, the plasma membrane in pancreatic islet β-cells (Rutter, 2001, 2004). We have recently shown that insulin-containing vesicles are transported from the cell center to the cortex primarily on the microtubule (MT)-based motor protein conventional kinesin, also called kinesin I (Varadi *et al*., 2002, 2003). By contrast, the short-range movements in the cortical regions of the cell that carry vesicles over the last few hundred nanometers to the cell surface seem more likely to involve F-actin, which is abundant in this region (Nakata and Hirokawa, 1992; Varadi *et al*., 2003; Tsuboi *et al*., 2003). Prime candidates for transport along these filaments are class V myosin motors (Mermall *et al*., 1998; Rudolf *et al*., 2003). Myosin Va (MyoVa) is composed of two heavy chains that dimerize via a coiled-coil motif located in the stalk region of the heavy chain (Cheney *et al*., 1993). The heavy chain contains an amino-terminal, actin-binding motor domain (Cheney *et al*., 1993) followed by a neck region to which up to six regulatory light chains are bound, and a carboxy-terminal globular domain (Cheney *et al*., 1993) that is thought to mediate organelle binding specificity (Reck-Peterson *et al*., 2000).

Insight into the potential functions of MyoVa has come from several lines of investigation, including identification of organelles and proteins that interact with MyoVa (Reck-Peterson *et al*., 2000; Karcher *et al*., 2002; Langford, 2002). The most powerful strategy has been the phenotypic characterization of lethal alleles of the *dilute* (MyoVa lethal mutant) mouse and cells derived from them (Mercer *et al*., 1991). The *dilute* mice develop severe seizures and die within 3 wk after birth. The primary neuronal defect thought be responsible is the absence of smooth endoplasmic reticulum within the dendritic spines of Purkinje neurons (Takagishi *et al*., 1996). Analyses of organelle movement in cultured melanocytes (Provance *et al*., 1996; Wu *et al*., 1998), neurons (Bridgman, 1999) and macrophages (Al Haddad *et al*., 2001) from *dilute* and wild-type mice also have provided evidence for a direct role of MyoVa in both organelle transport and tethering. Moreover, MyoVa has been identified on synaptic vesicles (Evans *et al*., 1998; Miller and Sheetz, 2000), and inhibition of myosin ATPase activity reduces neurotransmitter release in brain slices (Prekeris and Terrian, 1997). In addition, a recent report revealed the role of MyoVa in the distribution of secretory granules in PC12 cells (Rudolf *et al*., 2003). Finally, the yeast homologue of MyoV, Myo2p, is involved in secretory vesicle (Schott *et al*., 1999), peroxisome (Hoepfner *et al*., 2001), and vacuole (Ishikawa *et al*., 2003) transport.

The role of MyoVa in mitochondrial transport is, however, less clear. In vitro motility assay demonstrated that actin-dependent motor activity is associated with mitochondria (Simon *et al*., 1995). Immunoelectron microscopy revealed association of MyoVa with the mitochondrial membrane in

This article was published online ahead of print in *MBC in Press* (http://www.molbiolcell.org/cgi/doi/10.1091/mbc.E04–11–1001) on March 23, 2005.

[V] The online version of this article contains supplemental material at *MBC Online* (http://www.molbiolcell.org).

Address correspondence to: Aniko Varadi (Aniko.Varadi@uwe.ac.uk) or Guy A. Rutter (g.a.rutter@bris.ac.uk).

Abbreviations used: $[Ca^{2+}]_i$, intracellular free calcium ion concentration; ER, endoplasmic reticulum; EGFP, enhanced green fluorescent protein; FACS, fluorescence activated cell sorting; KRH, Krebs-Ringer-HEPES; LDCV, large dense core vesicle (secretory granule); MGTD, myosin Va globular tail domain; MT, microtubule; MyoVa, myosin Va; NPY, neuropeptide Y; siRNA, small interfering RNA; TIRF, total internal reflection fluorescence.

melanoma cells (Nascimento *et al*., 1997). Furthermore, a recent study also described the presence of this motor protein on mitochondria in myoblasts and suggested a role for MyoVa in calcium-dependent movements of these organelles (Yi *et al*., 2004). In contrast, mitochondrial transport was not affected in cells bearing mutations in either of the genes for myosins I, II, and V (DePina and Langford, 1999), and a shortening of the lever arm of Myo2p had no effect on mitochondrial morphology, actin organization, or the rate of mitochondrial movement in the mother cell (Boldogh *et al*., 1998). On the other hand, Myo2p mutant cells were defective in the segregation of mitochondria (Boldogh *et al*., 1998, 2004; Itoh *et al*., 2002).

Myosin Va is recruited to the vesicle surface by members of the Rab family of G proteins (Fukuda *et al*., 2002; Hume *et al*., 2002; Provance *et al*., 2002, Wu *et al*., 2002b). This process requires the presence of a rabphilin-like effector protein that bridges the indirect interaction between the Rab protein and myosin Va (Wu *et al*., 2002a; Fukuda *et al*., 2002). In melanocytes, Rab27a binds to the melanosome first and then recruits melanophilin/Slac-2a, a rabphilin-like effector protein, which in turn recruits myosin Va (Fukuda *et al*., 2002; Wu *et al*., 2002a,b). In pancreatic β-cells, suppression of Rab27a function impaired insulin exocytosis triggered by secretagogues (Waselle *et al*., 2003). The β-cells also express a Rab27a effector protein granuphilin-a/SLP4-a, which is localized on the membrane of insulin granules (Wang *et al*., 1999; Yi *et al*., 2002; Izumi *et al*., 2003), and its overexpression causes a profound inhibition of depolarization-induced insulin secretion (Wang *et al*., 1999; Coppola *et al*., 2002; Torii *et al*., 2002). Granuphilin directly binds to syntaxin 1a (Torii *et al*., 2002, 2004) and Munc 18-1 (Coppola *et al*., 2002) and is thought to be involved in tethering insulin granules to the plasma membrane (Torii *et al*., 2004). MyRIP/Slac2c, another Rab27a effector (Kuroda *et al*., 2002), is also expressed in β-cells and involved in the regulation of insulin release (Waselle *et al*., 2003). However, unlike for Rab27 or its effector proteins, the role of MyoVa in insulin-containing vesicle transport and membrane fusion is not known.

Here, we investigated the involvement of MyoVa in the distribution, motility, and exocytosis of insulin-containing vesicles in single pancreatic β-cells (MIN6). Inhibition of MyoVa function achieved by RNA interference or overexpression of a dominant-negative mutant resulted in clustering of secretory granules, a substantial reduction in the number of vesicles docked at the plasma membrane, and a decrease in the number of single exocytotic events and in global insulin release. These data demonstrate that MyoVa is essential for trafficking secretory organelles in neuroendocrine cells.

MATERIALS AND METHODS

Materials

Cell culture reagents were from Invitrogen (Life Science Research, Paisley, United Kingdom), and all molecular biologicals were from Roche Diagnostics (Lewes, United Kingdom). Alexa Fluor goat anti-rabbit or anti-guinea pig 488 and 568 secondary antibodies and Alexa Fluor 488-phalloidin were from Molecular Probes (Eugene, OR). Mouse monoclonal anti-α-tubulin was obtained from Sigma Chemical (Poole, Dorset, United Kingdom). Rabbit polyclonal anti-myosin Va antibody, DIL2, was raised against a glutathione *S*-transferase (GST)-fusion protein containing myosin V heavy chain residues 910-1106, which correspond to the first segment of α-helical coiled-coil in the central rod domain (Wu *et al*., 1998).

Cell Culture

MIN6 pancreatic β-cells (passages 19–35) were cultured in DMEM supplemented with 15% (vol/vol) fetal calf serum, 100 U ml^{-1} penicillin, 0.1 mg ml^{-1} streptomycin, and 2 mM L-glutamine at 37°C in an atmosphere of humidified air (95%) and CO_2 (5%) as described previously (Molnar *et al*., 1995).

Plasmids

A plasmid encoding mitochondrially targeted *Discoideum* red fluorescent protein (Mito.DsRed) was generated as described previously (Varadi *et al*., 2002). The expression vector myosin Va globular tail domain (MGTD).pEGFP was described previously (Wu *et al*., 1998). Plasmid encoding neuropeptide Y (NPY)-targeted monomeric red fluorescent protein (NPY-mRFP) was generated as described previously (Tsuboi *et al*., 2003).

RNA Preparation, Reverse Transcription, and PCR

Total RNA from mouse brain, spleen, and MIN6 pancreatic β-cells was prepared as described previously (Varadi *et al*., 1996). The total RNA (3 μg) was reverse transcribed at 42°C for 60 min in 50 μl of reaction mixture containing 1× reverse transcriptase buffer (50 mM Tris-HCl, pH 8.3, 40 mM KCl, 1 mM dithiothreitol [DTT], and 6 mM $MgCl_2$) containing 1.25 μg of oligo(dT), 0.5 mM each dNTP, 10 mM DTT, 40 U of rRNasin, and 500 U of Moloney murine leukemia virus reverse transcriptase. One-tenth of the cDNA was subjected to a PCR in 50-μl reaction mixture containing 1× PCR buffer (50 mM KCl, 10 mM Tris-HCl, pH 9.0, and 5 mM DTT), which contained 2 or 4 mM $MgCl_2$, 0.1 mM each dNTP, 20 pmol of each primer, and 0.5 U of *Taq* DNA polymerase (Promega, Madison, WI). PCR was carried out in a programmable thermal controller (PTC-100; MJ Research, Essex, United Kingdom) at 95°C for 2 min followed by 30 cycles at 95°C for 1 min, 53°C for 1 min, and 72°C for 1 min. The last cycle was followed by a final extension step at 72°C for 10 min. After PCR, the samples were subjected to electrophoresis in a 1.9% (wt/vol) agarose gel containing 0.4 μg of ethidium bromide in 1× TBE buffer (89 mM Tris base, 89 mM boric acid, and 2 mM EDTA). For DNA sequencing and restriction enzyme digestion, 100-μl PCR samples were precipitated with ethanol and then fractionated by electrophoresis in 1.3% (wt/vol) low melting point agarose gels. The separated bands were isolated, and the PCR products were extracted from the gel slices by Wizard PCR preps DNA purification system (Promega). The primers were designed to flank the alternative spliced forms in the C-terminal tail domain of MyoVa (Seperack *et al*., 1995). The following forward 1) 5′-CGAGCTGAATGAGTTGCGC-3′, nucleotides 3700–3718; 2) 5′-CATCTTGAGGTCGCAGCTGG-3′, nucleotides 3841–3860; and reverse 3) 5′-GATATGTTCTCCATCTGCC-3′, nucleotides 4371–4389; 4) 5′-GCTCATCGATGATCTCTCCTG-3, nucleotides 4392–4412, primers were used. Numbers correspond to MyoVa cDNA accession number NM_010864. We used these primers in combinations (1–3, 1–4, 2–3, and 2–4), and all PCR reactions resulted in identical alternative spliced forms in all samples tested. PCR amplification of MyoVa with primers 1 and 3 are shown on Figure 1A. The following controls were used to check for possible amplification of contaminant DNA and RNA by PCR: RNA blanks taken through the cDNA step in the absence of reverse transcriptase were used in every PCR reaction and for each set of primers; samples without templates were run for every primer pair for each PCR experiment.

Live Cell Imaging and Immunocytochemistry

Cells were cotransfected with 1 μg of plasmids encoding 1) MGTD.EGFP and NPY.mRFP, 2) MGTD.EGFP and Mito.DsRed; or 3) empty vectors (pAdTrack-CMV, the latter encodes enhanced green fluorescent protein [EGFP]) (He *et al*., 1998), by using 10 μg ml^{-1} LipofectAMINE in Opti-MEM I medium (Invitrogen) for 4 h. For live imaging, a Nipkov disk-based UltraVIEW confocal system (PerkinElmer Life and Analytical Sciences, Boston, MA) was used at 2–4 Hz for 100 s (200–400 frames in total) in Krebs-Ringer-HEPES (KRH) bicarbonate buffer composed of 140 mM NaCl, 3.6 mM KCl, 0.5 mM NaH_2PO_4, 0.5 mM $MgSO_4$, 2.0 mM $NaHCO_3$, 16–30 mM glucose, 10 mM HEPES, pH 7.4, and 1.0 mM $CaCl_2$ equilibrated with O_2/CO_2 [95:5 (vol/vol)] at 37°C. Immunocytochemistry was performed as described previously (Varadi and Rutter, 2002), and then images were captured on an UltraVIEW confocal microscope (Varadi *et al*., 2004).

Total Internal Reflection Fluorescence (TIRF) Microscopy

Cells were imaged in KRH bicarbonate buffer initially at 3 mM and then at 30 mM glucose. Incubations were performed on a thermostatically controlled (37°C) stage of an Olympus IX-70 microscope (Olympus UK, London, United Kingdom) fitted with a high numerical aperture objective lens (Apochromatic, 100×, 1.65 numerical aperture, infinity corrected; Olympus UK). To assess the dynamics of NPY.mRFP, we used a TIRF microscope (Till Photonics, Munich, Germany) as described previously (Tsuboi *et al*., 2000; Pinton *et al*., 2002; Tsuboi and Rutter, 2003). Images were captured at 2 Hz with a cooled charge-coupled device camera (640 × 480 pixels, IMAGO; Till Photonics) controlled by TillvislON software. Image analysis was performed with MetaMorph software (Universal Imaging, Downingtown, PA).

Measurement of Intracellular Free Ca^{2+} Concentration $[Ca^{2+}]_i$

Changes in $[Ca^{2+}]_i$ were measured at 37°C with entrapped Fura-2 (Grynkiewicz *et al*., 1985) by using a Leica DM-IRBI inverted microscope (40×

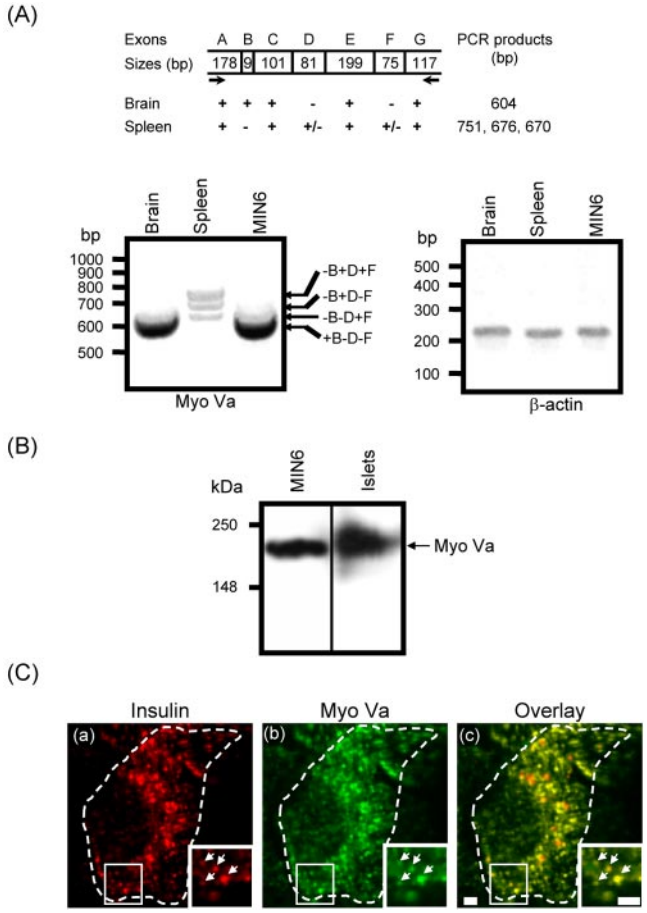

Figure 1. MyoVa is expressed in MIN6 cells and colocalized with insulin-containing vesicles. (A) The different alternative spliced forms of MyoVa were amplified by PCR. The structure of the possible alternative spliced forms is shown at the top. The capital letters represent exons as described previously (Seperack *et al*., 1995). The bold arrows represent the primer set used in RT-PCR amplification. Agarose gels show the MyoVa and β-actin amplification products from brain, spleen, and MIN6 cells. (B) Homogenates from MIN6 and primary rat pancreatic islet cells were prepared and proteins separated on by SDS gel chromatography (see *Materials and Methods*). Immunoblots were probed with a rabbit polyclonal anti-MyoVa antibody (DIL2, 1:5000 dilution). (C) MIN6 cells were fixed and coimmunostained with a rabbit polyclonal anti-MyoVa (1:1000 dilution) and a guinea pig polyclonal anti-insulin (1:1000 dilution) primary antibody then visualized with an Alexa Fluor goat anti-guinea pig 568 (a) and an Alexa Fluor goat anti-rabbit 488 (b) secondary antibody, respectively. (c) Overlay of a and b. Arrows indicate colocalization of insulin and MyoVa on individual vesicles. Hatched boundaries obtained from overlay with the transmitted image of the cell, indicate the cell periphery. Zoomed in regions are shown on the inserted images.

objective) and a Hamamatsu C4742-995 charged-coupled device camera driven by OpenLab software (Improvision, Coventry, United Kingdom) (Varadi and Rutter, 2002).

Silencing of Endogenous Myosin Va Expression with Small Interfering RNAs (siRNAs)

Sequences corresponding to the mouse myosin Va cDNA (Strobel *et al*., 1990) 2390–2410, 5′-AAGAGATACCTGTGTATGCAG-3′; and 2507–2528, 5′-AAGTACTGGCGCATGTATGTG-3′) were used as targets for siRNA. The following siRNAs were used as controls: 5′-AAGTGTGCAACCATGTGAATG-3′ and 5′-AAGTGGTTGGCGATTACCGAT-3′. These sequences showed no significant homology to any other gene known analyzed using BLAST search. siRNAs were synthesized by in vitro transcription by using the Silencer siRNA construction kit (Ambion, Austin, TX). MIN6 cells were transfected with 60 pmol of siRNA duplex by using 3 μl of Oligofectamine (Invitrogen) in growth medium without antibiotics or serum for 5 h (Varadi *et al*., 2003). Whole cell lysate was prepared 24, 48, 72, and 96 h after transfection. Cell lysate (10 μg) from siRNA and control RNA-transfected cells were separated on a 9% polyacrylamide gel and then blotted onto Immobilon-P transfer membrane and probed with a rabbit polyclonal anti-myosin Va antibody and a mouse monoclonal anti-tubulin antibody. The blots were scanned and quantified with NIH ImageJ software (http://rsb.info.nih.gov/ij/).

Assay of Insulin Release

MIN6 cells were seeded at a density of $4–6 \times 10^5$ ml^{-1} on 24-mm-diameter poly-L-lysine–coated coverslips and cultured overnight. Cells were transfected with siRNAs as described above. The cells were cultured for 48 h, and insulin release was stimulated and assayed as described previously (Varadi *et al*., 2002) using Mercodia ultrasensitive mouse insulin enzyme-linked immunosorbent assay (ELISA) kit (Mercodia AB, Uppsala, Sweden).

Subcellular Fractionation by Using OptiPrep Density Gradient Centrifugation

Cells were homogenized in a buffer containing 0.3 M sucrose, 1 mM EDTA, 1 mM $MgSO_4$, 10 mM MES-NaOH, pH 6.5, 1 mM phenylmethylsulfonyl fluoride (PMSF), 5 μg ml^{-1} aprotinin, and 5 μg ml^{-1} leupeptin by using a ball-bearing homogenizer and then centrifuged at $500 \times g$ for 10 min. The postnuclear supernatant was layered on top of a continuous 8–19% (wt/vol) OptiPrep gradient obtained using a Gradient Master (BioComp Instruments, Fredericton, New Brunswick, Canada) and centrifuged at $16,000 \times g$ for 16 h. Gradient fractions were collected by downward displacement (Gradient station; BioComp Instruments).

Fluorescence-activated Cell Sorting (FACS) of Vesicles and Precipitation with Trichloroacetic Acid (TCA)

MIN6 cells were infected with the recombinant phogrin.EGFP adenoviral construct at a multiplicity of 30–100 viral particles/cell, for 1 h. Cells were subsequently used 24 h postinfection when >95% of cells were infected. Cells were scraped into ice-cold buffer containing 10 mM 3-(*N*-morpholino)propanesulfonic acid (MOPS), 260 mM sucrose, pH 6.5, 1 mM PMSF, 5 μg ml^{-1} aprotinin, and 5 μg ml^{-1} leupeptin and then homogenized with a Teflon homogenizer and centrifuged at $500 \times g$ for 5 min. The postnuclear supernatant was resuspended in MOPS buffer to a concentration of 1–2 mg ml^{-1} and sorted into two fractions: particles labeled with EGFP and unlabeled organelles. Sorting was carried out on a FACS Vantage sorter (BD Biosciences, San Jose, CA) fitted with a 488-nm argon ion laser. The EGFP fluorescence was measured using a band pass filter at 530/30 nm. Vesicles (7×10^6) were obtained following sorting. Vesicles (7×10^4) were seeded onto poly-L-lysine–coated coverslips and used for immunocytochemistry. The remaining vesicle suspension was treated with equal volume of 20% (vol/vol) TCA for 30 min at 4°C and then centrifuged at $13,000 \times g$ for 10 min. The pellet was washed twice with cold acetone and then dried. The proteins were separated on SDS-gels.

Statistical Analysis

Data are presented as the mean ± SEM for the number of observations given, and statistical significance was calculated using an unpaired Student's *t* test.

RESULTS

Myosin Va Is Expressed in Clonal MIN β-Cells and Is Associated with Insulin-containing Vesicles

Insulin-containing vesicles undergo short (non-Brownian) movements in the F-actin–rich cell cortex in clonal MIN6 pancreatic β-cells (Tsuboi *et al*., 2003). To investigate whether this movement might involve F-actin–dependent transport via myosin motors, we investigated the presence of unconventional MyoVa on insulin-containing LDCVs.

First, we investigated the expression of MyoVa mRNA in MIN6 β-cells by using reverse transcription (RT)-PCR. A strategy was used by which the four different alternatively spliced isoforms of MyoVa could be identified (Figure 1A; -B+D+F, -B+D-F, -B-D+F, and +B-D-F). Spleen is known to express three splice variants of MyoVa (Figure 1A; -B+D+F, -B+D-F, -B-D+F; Seperack *et al*., 1995; Huang *et al*., 1998a,b; Au and Huang, 2002). The forth and shortest splice form, excluding both exons D and F,′ is expressed in

brain (Figure 1A; +B-D-F; Seperack *et al*., 1995; Huang *et al*., 1998a,b ; Au and Huang, 2002). Similar to brain and other neuroendocrine cells (Seperack *et al*., 1995; Nagashima *et al*., 2002; Wu *et al*., 2002b), MIN6 β-cells expressed only the +B-D-F splice variant (Figure 1A). Immunoblot analysis revealed that MyoVa is present at the protein level in both MIN6 β-cells and primary rat islets of Langerhans (Figure 1B). By using double-immunofluorescent microscopy, MyoVa was localized principally on insulin-positive structures in both MIN6 cells (Figure 1C, zoomed in regions, arrowheads) and in primary rat β-cells (our unpublished data).

To assess the proportion of cellular MyoVa that was stably associated with LDCs, we next explored the behavior of MyoVa and other organelle markers upon density gradient fractionation of extracts from clonal MIN6 β-cells. Secretory granules were enriched from the postnuclear supernatant by differential centrifugation and subsequently loaded onto a continuous OptiPrep density gradient to separate the vesicular components according to their buoyant density. The obtained gradient fractions were analyzed by immunoblotting to determine the distribution of MyoVa (Figure 2A, MyoVa), glycerol phosphate dehydrogenase (mGPDH; a marker protein for mitochondria; Figure 2A), phogrin (LDCV membranes) (Wasmeier and Hutton, 1996; Pouli *et al*., 1998); *trans*-Golgi network protein 38 (TGN38; Golgi) (Luzio *et al*., 1990); insulin receptor (plasma membrane [PM]); mannose-6-phosphate receptor (lysosomes), and sterol regulatory element binding protein 1c precursor (endoplasmic reticulum [ER]; Varadi and Rutter, unpublished data) (Brown and Goldstein, 1997). The distribution of various organelles detected with organelle-specific antibodies, or by the measurement of insulin content of each fraction, is indicated in Figure 2A. By this approach, the peak of MyoVa immunoreactivity (Figure 2A, fractions 9–12) coincided closely with that of insulin (Figure 2A, fractions 10–12) and of the vesicle transmembrane protein phogrin (fractions 10–12; our unpublished data). In contrast, only a very small proportion of the total MyoVa immunoreactivity was found in the cytosolic (Figure 2A, fractions 1–4), ER (Figure 2A, fractions 2 and 3), mitochondrial (Figure 2A, fractions 13–15), or other fractions.

Because the lighter insulin-containing fractions also possessed Golgi-derived membranes, we sought further to demonstrate the association of MyoVa with insulin-containing vesicles by FACS phogrin-EGFP–labeled vesicles. Phogrin-EGFP provides an efficient and selective tag for LDCVs, as demonstrated by the close (>95%) colocalization of phogrin-EGFP and insulin in this cell type (Pouli *et al*., 1998; Varadi *et al*., 2002; Tsuboi and Rutter, 2003). FACS-purified phogrin-EGFP–labeled particles were positive for both insulin (Figure 2B, a–c) and MyoVa (Figure 2B, d–f), and the apparent dimensions of the doubly labeled structures (200–500 nm) corresponded closely with those of dense-core secretory vesicles (Figure 2B) (Bonner-Weir, 1988), at least at the limit of light microscopy. To eliminate the possibility that the MyoVa antibody nonspecifically cross-reacted with insulin when used for immunocytochemistry, we precipitated the FACS-sorted vesicles with trichloroacetic acid, immunoblotted, and then probed with the MyoVa-specific antibody. This antibody recognized MyoVa with the correct molecular weight in these samples (Figure 2B, arrow). Together, the three complimentary approaches used above support the view that the majority of MyoVa is associated with insulin-containing granules in β-cells.

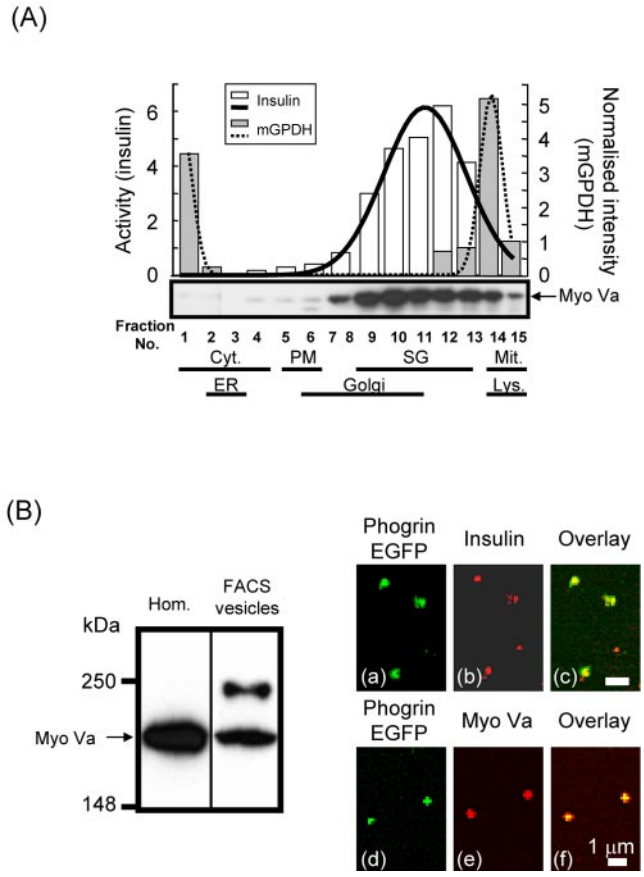

Figure 2. MyoVa is associated with insulin-containing vesicle fraction. (A) MIN6 cell homogenates were fractionated by OptiPrep density gradient centrifugation and the insulin content in each fraction was determined (see *Materials and Methods*). The same subcellular fractions were separated by SDS gel electrophoresis and the immunoblots probed with a rabbit polyclonal anti-MyoVa antibody (1:5000 dilution) or with a rabbit polyclonal anti-glycerol phosphate dehydrogenase (mGPDH, 1:1000 dilution) antibody. The latter was used to detect mitochondria. The amount of insulin and mGPDH was normalized to the protein content in each fraction. The continuous and dotted lines represent the Gaussian distribution of insulin and mGPDH, respectively. Distribution of various organelles in each fraction detected by organelle specific antibodies (*see Materials and Methods* for details) is indicated at the bottom. Cyt., cytosol; Lys., lysosomes SG, secretory granules (LDCVs); Mit., mitochondria. (B) MIN6 cells were infected with the recombinant phogrin.EGFP adenoviral construct and fluorescent EGFP-labeled vesicles were separated from nonlabeled organelles by FACS sorting. The sorted vesicle proteins (8×10^6 fluorescent particles) were precipitated with TCA and then separated on a SDS gel. The immunoblot was probed with the rabbit polyclonal anti-MyoVa antibody (1:5000 dilution). Arrow on the left indicates the presence of MyoVa in the cell homogenate (Hom.) and the FACS sorted vesicles (FACS vesicles). FACS sorted vesicles were seeded onto poly-L-lysine–coated coverslips and immunostained with a guinea pig anti-insulin antibody or a rabbit polyclonal anti-MyoVa antibody then visualized with an Alexa Fluor goat anti-guinea pig 568 (a) and an Alexa Fluor goat anti rabbit 568 (b) secondary antibody, respectively. (a and d) Phogrin.EGFP fluorescence. (c and f) Overlay of a and b and d and e, respectively.

Expression of the MyoVa Tail Domain Leads to Clustering of Insulin-containing Vesicles

To test whether inhibition of the motor activity of MyoVa leads to reduction in motility and distribution of insulin-

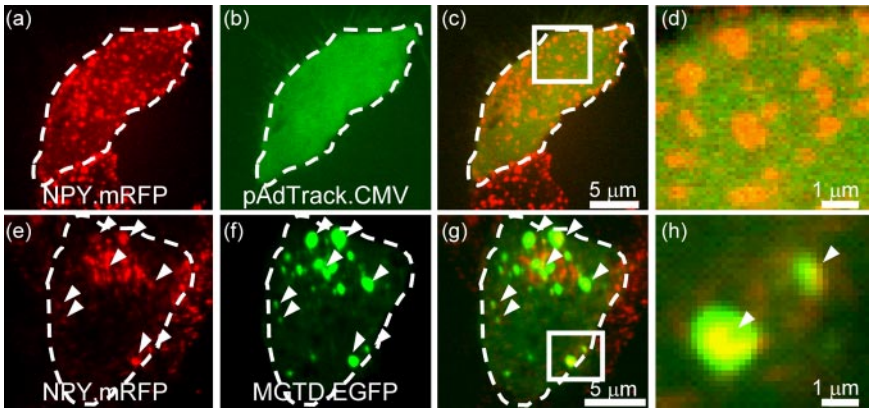

Figure 3. Overexpression of MGTD inhibits cortical localization of secretory granules and induces the formation of secretory granule clusters. MIN6 cells were cotransfected with NPY.mRFP and MGTD.EGFP or the empty plasmid pAdTrack.CMV and then imaged on the UltraVIEW live cell confocal imaging system (see *Materials and Methods* for details). (a and e) NPY.mRFP fluorescence. (b and f) EGFP fluorescence. (c and g) Overlay of a and b and e and f, respectively. (d and h) Zoomed in regions in c and g, respectively.

containing vesicles, we transfected a C-terminal tail fragment of MyoVa, MGTD.EGFP, into β-cells. This tail fragment is known to act as a potent inhibitor of MyoVa function in mouse melanocytes (Wu *et al*., 1998) and PC12 cells (Rudolf *et al*., 2003). We labeled insulin-containing vesicles by expressing cDNA encoding neuropeptide Y fused to monomeric red fluorescent protein (NPY.mRFP), a construct that is targeted efficiently to LDCVs (Tsuboi and Rutter, 2003). Whereas in control cells labeled secretory vesicles were evenly distributed and frequently seen at the cell periphery (Figure 3, a–d), expression of the MyoVa tail fragment led to vesicle clustering and exclusion from the cell cortex (Figures 3, e–h, and 4, a–d). If MGTD.EGFP directly interacted with secretory granules, then we expected to observe an increased local concentration of MGTD.EGFP in the clusters of fluorescent secretory vesicles. As anticipated, MGTD.EGFP also showed strong clustering (Figure 3f) and high, although not complete, colocalization with the accumulated red fluorescence of vesicles (Figure 3, g and h). The observed formation of clusters is likely to involve both a block of transport of LDCVs to the actin cortex and/or a change in tethering. Both phenomena have previously been observed for melanosomes in melanocytes expressing the tail fragment of MyoVa and are also apparent in melanocytes from *dilute* mice that carry a homozygous mutation in the MyoVa gene (Wu *et al*., 1998).

In cells where more moderate clustering was apparent, we were able to show clear colocalization of single vesicles with MGTD.EGFP (Figure 4A, a–d, and Fig 4Acvideo1.mov). Although it was not feasible to analyze individual vesicle movements in cells where intense clustering was seen (Figure 3), this was possible in cells with moderate vesicle clustering. As shown in Figure 4B (Fig 4Bvideo2.mov), vesicles frequently moved together with the MGTD.EGFP, strongly suggesting that MGTD.EGFP was bound to vesicles.

Impact of MyoVa Inhibition on Mitochondrial Movements and the Cytoskeleton

In contrast to the situation with LDCVs, coexpression of MGTD.EGFP with Mito.DsRed did not induce any cluster-

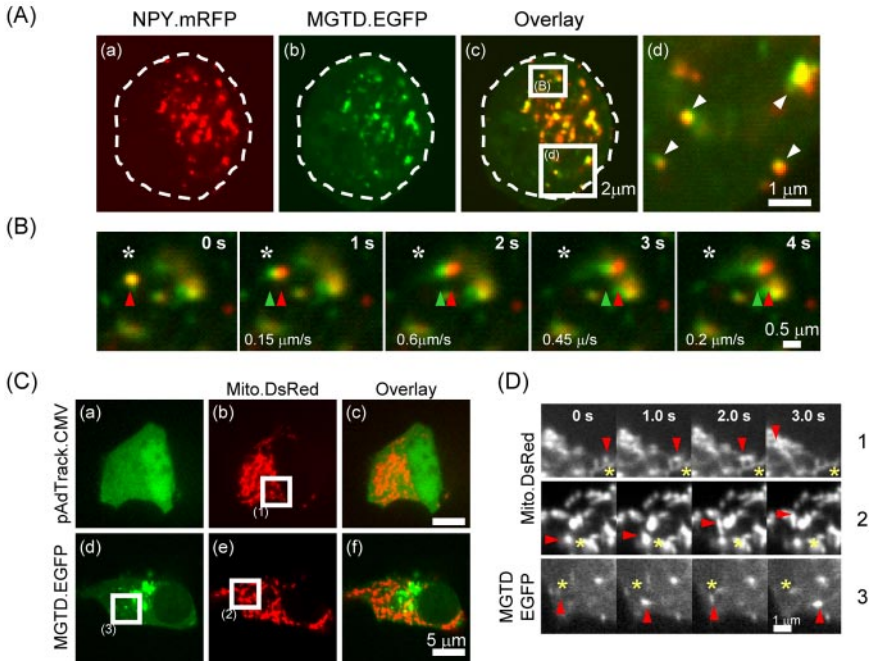

Figure 4. MGTD colocalizes and moves with secretory granules. MIN6 cells were cotransfected with NPY.mRFP and MGTD.EGFP and then imaged on the UltraVIEW life cell confocal imaging system at 4 Hz. (a) NPY.mRFP fluorescence. (b) MGTD.EGFP fluorescence. (c) Overlay of a and b. (B, d) Zoomed in regions in c, as indicated. (B) Movements of NPY.mRFP and MGTD.EGFP were imaged sequentially with a 250-ms delay between channels. The velocity of both structures was calculated using the image analysis software MetaMorph (Universal Imaging) and is shown on the images. Indicated by the red and green arrowheads is a single NPY.mRFP-labeled vesicle and MGTD.EGFP, respectively. The original starting position is indicated with a white asterisk. Direction of movement is labeled by yellow arrows (see Supplemental Data Fig 4Acvideo1.mov and Fig 4Bvideo2.mov). (C) MIN6 cells were cotransfected with 1 μg of MGTD.EGFP or the empty vector pAdTrack.CMV and 0.25 μg of Mito.DsRed and 24 h later imaged on the UltraVIEW live cell confocal imaging system at 4 Hz. (a and d) EGFP fluorescence. (b and e) Mito.DsRed fluorescence. (c and f) Overlay of a and b and d and e, respectively. Boxed regions on b, d, and e are enlarged in C. (D) Indicated by a red arrowhead is a single moving mitochondrion (1 and 2) or MGTD.EGFP (3) whose original starting position is labeled with a yellow asterisk (see Supplemental Data Fig 4Acvideo1.mov and Fig 4Bvideo2.mov).

ing of mitochondria (Figure 4C) and the majority of the expressed MGTD.EGFP failed to localize with these organelles (Figure 4C, d–f). Moreover, the movement of individual mitochondria was not affected by expression of MGTD.EGFP (Figure 4, D and C). Thus, rapid movements of MGTD.EGFP were observed that did not coincide with those of the separately labeled mitochondria (Figure 4D).

To eliminate the possibility that the clustering of LDCVs may be due to altered organization of actin filaments and/or microtubules, we visualized these cytoskeletal structures in control and MGTD.EGFP-expressing cells. As anticipated given the normal mitochondrial distribution and motility, no apparent effect of MGTD.EGFP was observed on the structure and organization of actin and tubulin networks (our unpublished data). In MIN6 cells, strong phalloidin staining was observed predominantly at the cortical regions, whereas tubulin extended from the perinuclear region to the cortex (our unpublished data). As expected, a small proportion of vesicles, probably those that were docked at the plasma membrane, clearly localized close to the phalloidin-positive F-actin cortex (our unpublished data). The above-mentioned data suggest that the expression of tail fragment of MyoVa does not inhibit cellular membrane traffic in general but is selective for MyoVa-associated organelles and interferes with their F-actin–dependent transport in the cortex.

Silencing of MyoVa by RNA Interference, or Expression of the MyoVa Tail Domain, Reduces the Number of Secretory Vesicles Docked at the Plasma Membrane, the Number of Exocytotic Events, and Insulin Release Provoked by Glucose

To confirm and further quantitate the change in the number of vesicles at the cortex after inhibition of MyoVa with MGTD.EGFP (Figures 3 and 4), we visualized vesicles within ~100 nm of the plasma membrane by using TIRF microscopy (Axelrod, 1981; Tsuboi *et al*., 2000). We first counted the number of plasma membrane-associated vesicles in a 200-μm^2 area. This revealed that MGTD.EGFP overexpression significantly reduced (by 52.6%) the number of plasma membrane-docked vesicles (Figure 5, A and B). We then counted the total number of NPY.mRFP release events from cells expressing NPY.mRFP together with empty plasmid (pAdTrack.CMV) or plasmid bearing MGTD.GFP during incubation with 50 mM KCl. The number of NPY.mRFP release events was reduced by 86.9% in the MGTD.EGFP-expressing cells compared with controls (Figure 5C and Fig 5avideo3.mov and Fig 5bvideo4.mov), whereas glucose or KCl-stimulated increases in $[Ca^{2+}]_i$ were not altered (Figure 5D).

To avoid potential nonspecific effects of overexpression of MGTD.EGFP, and to permit measurements of insulin secretion in cell populations, we used RNA interference (Elbashir *et al*., 2001) to silence endogenous MyoVa expression in MIN6 β-cells (Varadi *et al*., 2003; Da Silva Xavier *et al*., 2004). We targeted two regions of mouse MyoVa cDNA (see *Materials and Methods*) and found that both of the siRNA duplexes tested reduced the total MyoVa expression by at least 40%. However the siRNA pair corresponding to 2390–2410 base pairs was more effective and reduced the total MyoVa expression by 55 ± 5% with respect to a scrambled oligonucleotide duplex; this siRNA was used in the experiments presented in Figure 6. In MyoVa-silenced cells, we found similar vesicle clustering as observed after MGTD.EGFP expression (Figure 6B, c and d vs. a and b; n = 315 cells in five independent experiments; n = 85 and 230 similar to those of image c and d, respectively), whereas significant

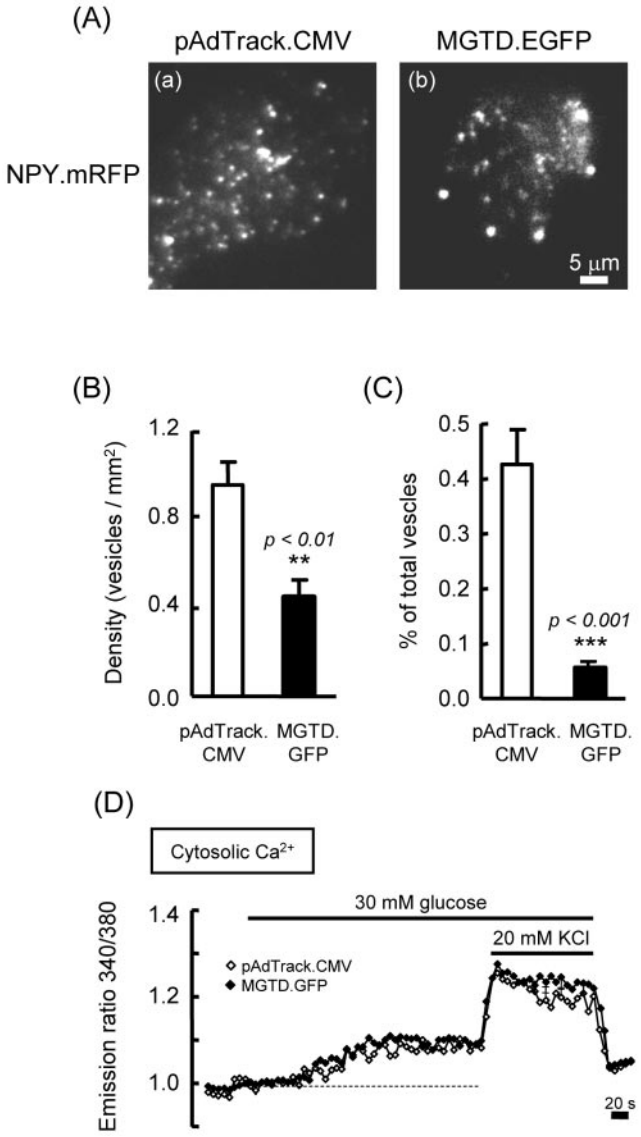

Figure 5. Blockage of MyoVa function reduces the number of plasma membrane-docked LDCVs and depolarization-induced exocytotic events. MIN6 cells were cotransfected with NPY.mRFP and MGTD.EGFP or the empty plasmid pAdTrack.CMV and then imaged by TIRF microscopy (*see Materials and Methods* for details). (A) Typical TIRF images of docked vesicles observed at 3 mM glucose in control (a) and MGTD.EGFP-overexpressing cells (b). (B) The density of docked vesicles was determined by counting the vesicles in each image (200-μm^2 area, n = 5 cells). (C) The number of NPY.mRFP release events was counted for 5 min and expressed as the percentage of the number of docked insulin vesicles. (D) $[Ca^{2+}]_i$ changes in control (open symbol, n = 158 cells in three independent experiments) and MGTD.EGFP-expressing cells (closed symbol, n = 58 cells in eight independent experiments) in response to stimulation with glucose or KCl (see Supplemental Data Fig 5avideo3.mov and Fig 5bvideo4.mov).

clustering of LDCVs was not detected in control cells (Figure 6B, a and b, n = 267 cells, in five independent experiments). As expected from previous transfection experiments in MIN6 cells (Varadi *et al*., 2002), the siRNA suppression of MyoVa protein expression was heterogeneous (Figure 6C). Thus, in 30–40% of the siRNA-treated cells endogenous MyoVa protein was no longer detectable (Figure 6C, ar-

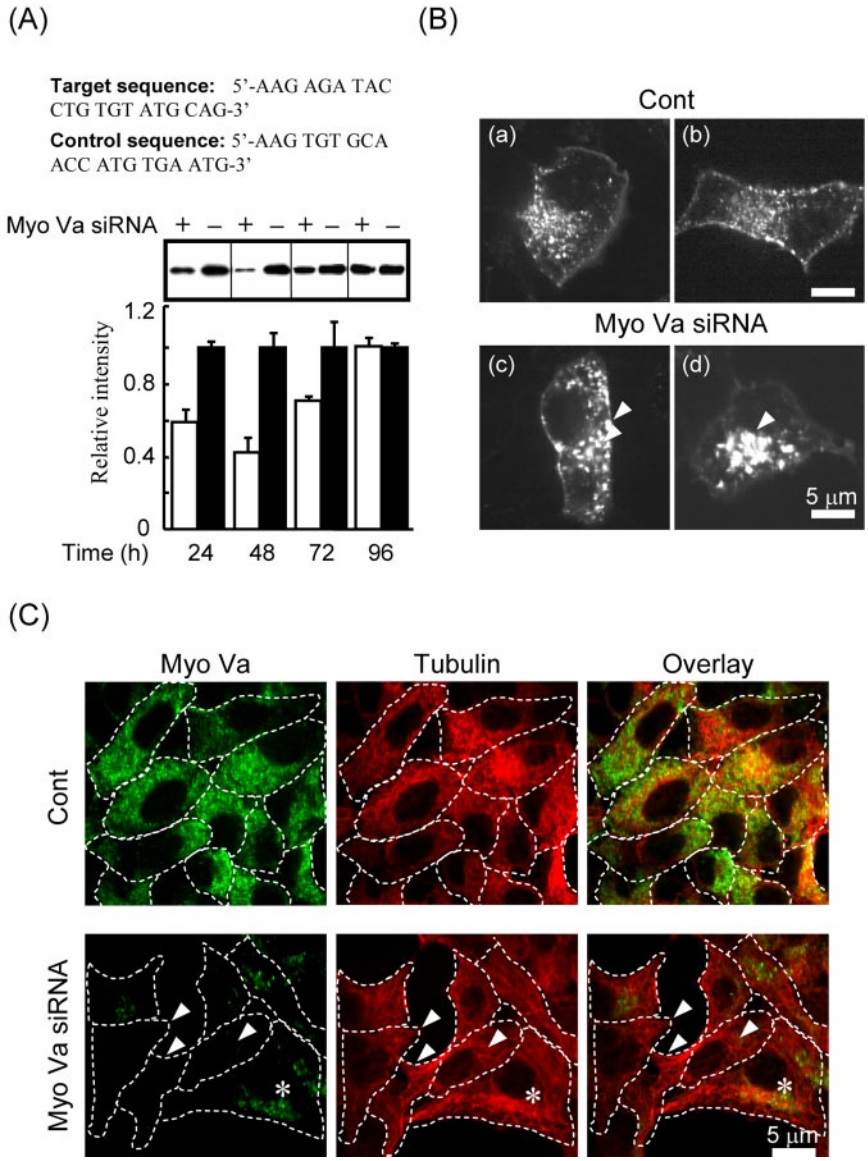

Figure 6. Silencing of endogenous MyoVa. (A) MIN6 cells were transfected with 60 pmol of anti-MyoVa or scrambled siRNAs (see *Materials and Methods*). Whole cell lysates were prepared 24, 48, 72, and 96 h after transfection. The immunoblot was probed with the anti-MyoVa antibody (1:5000), scanned, and quantified with NIH ImageJ software (http://rsb.info.nih.gov/ij/). Data show mean values ± SE of six independent transfections. (B) Cells were transfected with siRNA for 36 h then infected with phogrin.E-GFP adenoviral construct at a multiplicity of 30–100 viral particles cell^{-1} for a further 12 h. Imaging was performed as described in Figure 2. (C) siRNA and control cells were fixed and coimmunostained with a rabbit polyclonal anti-MyoVa antibody and a mouse monoclonal anti-tubulin antibody and then visualized with an Alexa Fluor goat anti-rabbit 488 (green) and an Alexa Fluor goat anti-mouse 568 (red) secondary antibody, respectively. Arrows and asterisk indicate cells in which no and some MyoVa staining were observed, respectively. Hatched boundaries obtained from overlay with the transmitted image of the cell indicate the cell periphery. Bars, 5 μm.

rows). By contrast, in the remainder of the cells, MyoVa expression was suppressed by 50–80%. We costained the cells for tubulin to eliminate the possibility that the observed reduction in MyoVa expression could be a result of uneven immunostaining. Excluding this possibility, tubulin staining was equally strong in the siRNA-treated cells as in control cells.

Insulin release was measured from MyoVa-silenced and control cells by using an insulin ELISA assay (see *Materials and Methods*). To investigate the effect of reduced MyoVa activity on the size of the readily releasable/docked vesicle pool (Bratanova-Tochkova *et al*., 2002; Rutter, 2004), we stimulated cells with KCl. Suppression of MyoVa activity lead to a 29 ± 3.4% decrease in the number of release events compared with control cells (Figure 7A). Similarly, glucose-stimulated insulin release, expected to reflect release of LDCVs from both a readily releasable and reserve pool, also was significantly reduced by 28 ± 5.7% (Figure 7B). These data are in agreement with those obtained by TIRF imaging, bearing in mind the heterogeneous suppression of total MyoVa after siRNA treatment. By contrast, the total insulin content of cells was identical under all conditions (picomoles per 500,000 cells; untransfected, 3.35 ± 0.11; control siRNA transfected, 3.21 ± 0.15; and siRNA transfected, 3.28 ± 0.09).

DISCUSSION

MyoVa Is a Mediator of Dense Core Vesicle Movement and Insulin Secretion

We provide here morphological and biochemical evidence that in pancreatic β-cells, a convenient neuroendocrine cell model, MyoVa 1) associates principally with secretory granules (Figures 1 and 2) and 2) transports these within the F-actin–rich cortex toward the plasma membrane. Thus, we show that suppression of MyoVa activity, achieved by two distinct means (use of a dominant-negative or RNAi) leads to clustering of vesicles and to a reduction in their cortical localization (Figures 3, 4, and 6 and Fig 4Acvideo1.mov). Although similar phenomena were reported recently in PC12 cells (Rudolf *et al*., 2003), the present report now provides functional data to demonstrate that changes in vesicle

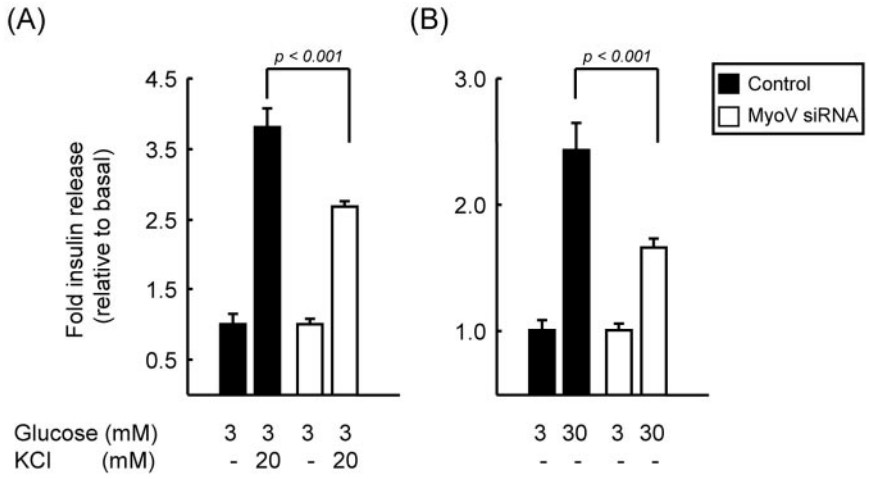

Figure 7. Suppressed expression of endogenous MyoVa inhibits glucose-stimulated insulin secretion. (A and B) Insulin release in control or anti-MyoVa siRNA-transfected cells was assayed with an insulin ELISA kit (see *Materials and Methods*). Data show mean values ± SE. The total insulin content of cells was identical under all conditions (per 500,000 cells; control, 3.35 ± 0.11 pmol; control siRNA transfected, 3.21 ± 0.15; and siRNA transfected, 3.28 ± 0.09).

distribution are accompanied by a significant reduction in the number of depolarization-stimulated exocytotic events and insulin release (Figures 5 and 7 and Fig 5avideo3.mov and Fig 5bvideo4.mov). In this way, we show that MyoVa-driven movements of vesicles along the cortical actin network are required for the terminal stages of regulated exocytosis.

In the present study, long excursions of individual LDCVs, likely to be dependent upon MTs (Pouli *et al*., 1998; Varadi *et al*., 2003), were observed in both dominant-negative MyoVa tail domain-expressing (Figure 4) and siRNA-silenced cells. This finding suggests that MT-dependent transport is unlikely to be strongly affected by the inactivation of MyoVa. Moreover, no apparent effect of expression of the dominant tail domain was observed on the structure and organization of the actin or tubulin networks (our unpublished data). Nevertheless, we cannot rule out the possibility that inhibition of MyoVa may have some impact on MT-dependent transport or structure (Weber *et al*., 2004). Furthermore, a recent report revealed that indeed MyoVa can mechanochemically couple MTs to F-actin in vitro (Cao *et al*., 2004) and implicated the tail domain in MT binding (Cao *et al*., 2004).

Role of MyoVa in Controlling Mitochondrial Movements

In contrast to the situation with LDCVs, we found no effect of inhibiting MyoVa activity on mitochondrial morphology or movement (Figure 4). In agreement with this observation, mitochondrial transport was not affected in cells bearing mutations in the genes for myosins I, II, and V (DePina and Langford, 1999). Furthermore, shortening of the lever arm of Myo2p, the mammalian homologue of myosin V in *Saccharomyces cerevisiae*, had no effect on mitochondrial morphology, actin organization, or the rate of mitochondrial movement in the mother cell (Boldogh *et al*., 1998), thus arguing against the role of MyoVa in mitochondrial motility during interphase. On the other hand, Myo2p mutant cells were defective in the segregation of mitochondria (Boldogh *et al*., 1998), suggesting that myosin family members may participate in mitochondrial movements under some circumstances, including mitosis. Furthermore, the results presented here do not support the model proposed recently by Hajnoczky and coworkers (Yi *et al*., 2004) in which MyoVa was suggested to be on mitochondrial membranes and involved in the Ca^{2+}-dependent control of mitochondrial motility.

Potential Mechanisms of MyoVa Recruitment to LDVCs

The finding of actin-based motor-dependent transport of secretory vesicles, together with previous observations showing an MT-dependent movement of secretory vesicles to the plasma membrane (Pouli *et al*., 1998; Varadi *et al*., 2002, 2003), provides strong evidence for the existence of a dual transport system used by LDCVs, which is likely to be dependent upon the localization of the vesicle within the cell. Evidence for such a dual transport system also has been provided for melanosomes (Reck-Peterson *et al*., 2000), the endoplasmic reticulum (Tabb *et al*., 1998; Reck-Peterson *et al*., 2000), and phagosomes (Al Haddad *et al*., 2001). Indeed, it seems that motor proteins associated with the surface of organelles are often organized into protein complexes (Schliwa, 1999). For example, a direct interaction between microtubule- and actin-based transport motors has been shown for the mouse ubiquitous kinesin heavy chain and MyoVa (Huang *et al*., 1999). Although the interaction between MyoVa and kinesin heavy chain might coordinate transport in several different ways, one appealing model (Huang *et al*., 1999) proposes that MyoVa and kinesin bind to the same cargo, as well as to each other, to form an integrated motor complex. In this model, the activity of the complex is tightly regulated such that only one motor in the complex is significantly active at any given time. The evident advantage of such a motor complex is that it may allow a single vesicle to be transported by multiple motors and to move on both MT and actin tracks. A vesicle thus equipped with multiple motors might make the transition from MT to actin filaments easily by switching between motor activities. In MT-rich cellular domains, it seems likely that kinesin activity would lead to long-range MT-based movement (Pouli *et al*., 1998; Varadi *et al*., 2002, 2003), whereas in regions such as the cellular cortex, where MTs are rare or absent, MyoVa would take over to deliver cargo to its final destination.

It is intriguing to ask how these complexes might be recruited to, and regulated on, LDCVs. Whereas kinectin is thought to mediate the binding of kinesin I to membranes (Vallee and Sheetz, 1996), more recent reports suggest that kinesin I binds to cargoes via a set of proteins, JIP-1, JIP-2, and JIP-3, also involved in intracellular signaling (Bowman *et al*., 2000; Verhey *et al*., 2001). For MyoVa, cytoplasmic domain of synaptobrevin-synaptophysin complex has been proposed to function as a binding partner on small synaptic vesicles (Prekeris and Terrian, 1997). On the other hand, the

small monomeric G protein family member Rab27a has been implicated in the interaction between melenosomes and MyoVa (Deacon and Gelfand, 2001) in a receptor-motor complex including the Rab27a binding protein melanophilin, a bridging protein with strong similarity to the Rab3a effector protein rabphilin (Matesic *et al*., 2001).

The interaction between melanophilin and MyoVa has been shown to be regulated by a melanocyte-specific alternative splicing in the tail domain of MyoVa. In MyoVa, alternative splicing takes place between exons A and G (Figure 1A) with four alternatively spliced isoforms containing different combinations of exons B, D, and F being identified (Huang *et al*., 1998a,b; Seperack *et al*., 1995). The presence of exon F, an alternatively spliced exon expressed in melanocytes but not in neuroendocrine cells, is required for MyoVa to localize to melanosomes (Seperack *et al*., 1995; Nagashima *et al*., 2002; Wu *et al*., 2002b). In addition, the globular tail domain is required for melanophilin–MyoVa interaction (Wu *et al*., 2002a). In PC12 cells, overexpression of a tail fragment containing exon F did not target to vesicular structures. However, the expression of exon B was required for the localization of MyoVa to vesicle structures in this neuroendocrine cell (Au and Huang, 2002). In agreement with these results, we found that the neuronal splice variant containing exon B but missing exons D and F is expressed in β-cells.

Given the above, it seems likely that exon B and the globular tail domain of MyoVa are involved in the interaction with a Rab effector protein in β-cells as described in melanosomes. However, the composition of the organelle receptor complex may well be different in the two cell types. Thus, Rab27a and MyRIP have been implicated in the regulation of exocytosis in pancreatic β-cells and neuroendocrine PC12 cells (Waselle *et al*., 2003, Desnos *et al*., 2003). However, the Rab27/MyRIP protein complex does not seem to require recruitment of myosin on the secretory granules for function (Waselle *et al*., 2003). The association of myosin Va and Rab27/MyRIP has not been demonstrated in vivo, although it contributes to the cytoplasmic distribution of secretory granules in PC12 cells (Rudolf *et al*., 2003). Might other members of the Rab family be involved in binding MyoVa to vesicles? Rab3a is known to be specifically associated with small synaptic vesicles and insulin granules (Regazzi *et al*., 1996) and thus may have a role, a view supported by the fact that Rab3a$^{-/-}$ mice develop of hyperglycemia and insulin secretory deficiencies (Yaekura *et al*., 2003). Further studies will be necessary to distinguish between these possibilities and to explore the mechanisms whereby increases in glucose concentration might lead to the recruitment of MyoVa to LDCVs in insulin-secreting cells.

ACKNOWLEDGMENTS

This study was supported by Wellcome Trust Programme Grant 067081/Z/02/Z and a Juvenile Diabetes Research Foundation Postdoctoral Fellowship (to T. T.). We thank Dr. Mark Jepson and Alan Leard (Bristol MRC Imaging Facility, University of Bristol, Bristol, United Kingdom) for technical assistance, Professor Peter Cullen for the use of the UltraVIEW confocal microscope, and Dr. Andrew Herman for the FACS of vesicles. We are grateful to Prof. V. Gelfand (University of Illinois, Urbana-Champaign, IL) for providing the MGTD.EGFP construct and DIL2 rabbit polyclonal anti-myosin V antibody. G.A.R. is a Wellcome Trust Research Leave Fellow.

REFERENCES

Al Haddad, A., *et al*. (2001). Myosin Va bound to phagosomes binds to F-actin and delays microtubule-dependent motility. Mol. Biol. Cell *12*, 2742–2755.

Au, J. S., and Huang, J. D. (2002). A tissue-specific exon of myosin Va is responsible for selective cargo binding in melanocytes. Cell Motil. Cytoskeleton *53*, 89–102.

Axelrod, D. (1981). Cell-substrate contacts illuminated by total internal reflection fluorescence. J. Cell Biol. *89*, 141–145.

Boldogh, I., Vojtov, N., Karmon, S., and Pon, L. A. (1998). Interaction between mitochondria and the actin cytoskeleton in budding yeast requires two integral mitochondrial outer membrane proteins, Mmm1p and Mdm10p. J. Cell Biol. *141*, 1371–1381.

Boldogh, I. R., Ramcharan, S. L., Yang, H. C., and Pon, L. A. (2004). A type V myosin (Myo2p) and a Rab-like G-protein (Ypt11p) are required for retention of newly inherited mitochondria in yeast cells during cell division. Mol. Biol. Cell *15*, 3994–4002.

Bonner-Weir, S. (1988). Morphological evidence for pancreatic polarity of beta cells within islets of Langerhans. Diabetes *37*, 616–621.

Bowman, A. B., Kamal, A., Ritchings, B. W., Philp, A. V., McGrail, M., Gindhart, J. G., and Goldstein, L. S. (2000). Kinesin-dependent axonal transport is mediated by the Sunday driver (SYD) protein. Cell *103*, 583–594.

Bratanova-Tochkova, T. K., Cheng, H., Daniel, S., Gunawardana, S., Liu, Y. J., Mulvaney-Musa, J., Schermerhorn, T., Straub, S. G., Yajima, H., and Sharp, G. W. (2002). Triggering and augmentation mechanisms, granule pools, and biphasic insulin secretion. Diabetes *51* (suppl 1), S83–S90, S83–S90.

Bridgman, P. C. (1999). Myosin Va movements in normal and dilute-lethal axons provide support for a dual filament motor complex. J. Cell Biol. *146*, 1045–1060.

Brown, M. S., and Goldstein, J. L. (1997). The SREBP pathway: regulation of cholesterol metabolism by proteolysis of a membrane-bound transcription factor. Cell *89*, 331–340.

Cao, T. T., Chang, W., Masters, S. E., and Mooseker, M. S. (2004). Myosin-Va binds to and mechanochemically couples microtubules to actin filaments. Mol. Biol. Cell *15*, 151–161.

Cheney, R. E., O'Shea, M. K., Heuser, J. E., Coelho, M. V., Wolenski, J. S., Espreafico, E. M., Forscher, P., Larson, R. E., and Mooseker, M. S. (1993). Brain myosin-V is a two-headed unconventional myosin with motor activity. Cell *75*, 13–23.

Coppola, T., Frantz, C., Perret-Menoud, V., Gattesco, S., Hirling, H., and Regazzi, R. (2002). Pancreatic beta-cell protein granuphilin binds Rab3 and Munc-18 and controls exocytosis. Mol. Biol. Cell *13*, 1906–1915.

Da Silva Xavier, G., Qian, Q., Cullen, P. J., and Rutter, G. A. (2004). Distinct roles for insulin and insulin-like growth factor-1 receptors in pancreatic beta-cell glucose sensing revealed by RNA silencing. Biochem. J. *377*, 149–158.

Deacon, S. W., and Gelfand, V. I. (2001). Of yeast, mice, and men. Rab proteins and organelle transport. J. Cell Biol. *152*, F21–F24.

DePina, A. S., and Langford, G. M. (1999). Vesicle transport: the role of actin filaments and myosin motors. Microsc. Res. Tech. *472*, 93–106.

Desnos, C., *et al*. (2003). Rab27A and its effector MyRIP link secretory granules to F-actin and control their motion towards release sites. J. Cell Biol. *163*, 559–570.

Elbashir, S. M., Harborth, J., Lendeckel, W., Yalcin, A., Weber, K., and Tuschl, T. (2001). Duplexes of 21-nucleotide RNAs mediate RNA interference in cultured mammalian cells. Nature *411*, 494–498.

Evans, L. L., Lee, A. J., Bridgman, P. C., and Mooseker, M. S. (1998). Vesicle-associated brain myosin-V can be activated to catalyze actin-based transport. J. Cell Sci. *111*, 2055–2066.

Fukuda, M., Kuroda, T. S., and Mikoshiba, K. (2002). Slac2-a/melanophilin, the missing link between Rab27 and myosin Va: implications of a tripartite protein complex for melanosome transport. J. Biol. Chem. *277*, 12432–12436.

Grynkiewicz, G., Poenie, M., and Tsien, R. Y. (1985). A new generation of Ca^{2+} indicators with greatly improved fluorescence properties. J. Biol. Chem. *260*, 3440–3450.

He, T. C., Zhou, S., da Costa, L. T., Yu, J., Kinzler, K. W., and Vogelstein, B. (1998). A simplified system for generating recombinant adenoviruses. Proc. Natl. Acad. Sci. USA *95*, 2509–2514.

Hoepfner, D., van den Berg, M., Philippsen, P., Tabak, H. F., and Hettema, E. H. (2001). A role for Vps1p, actin, and the Myo2p motor in peroxisome abundance and inheritance in *Saccharomyces cerevisiae*. J. Cell Biol. *155*, 979–990.

Huang, J. D., Cope, M. J., Mermall, V., Strobel, M. C., Kendrick-Jones, J., Russell, L. B., Mooseker, M. S., Copeland, N. G., and Jenkins, N. A. (1998a). Molecular genetic dissection of mouse unconventional myosin-VA: head region mutations. Genetics *148*, 1951–1961.

Huang, J. D., Mermall, V., Strobel, M. C., Russell, L. B., Mooseker, M. S., Copeland, N. G., and Jenkins, N. A. (1998b). Molecular genetic dissection of mouse unconventional myosin-VA: tail region mutations. Genetics *148*, 1963–1972.

Huang, J. D., Brady, S. T., Richards, B. W., Stenolen, D., Resau, J. H., Copeland, N. G., and Jenkins, N. A. (1999). Direct interaction of microtubule- and actin-based transport motors. Nature *397*, 267–270.

Hume, A. N., Collinson, L. M., Hopkins, C. R., Strom, M., Barral, D. C., Bossi, G., Griffiths, G. M., and Seabra, M. C. (2002). The leaden gene product is required with Rab27a to recruit myosin Va to melanosomes in melanocytes. Traffic *3*, 193–202.

Ishikawa, K., Catlett, N. L., Novak, J. L., Tang, F., Nau, J. J., and Weisman, L. S. (2003). Identification of an organelle-specific myosin V receptor. J. Cell Biol. *160*, 887–897.

Itoh, T., Watabe, A., Toh, E., and Matsui, Y. (2002). Complex formation with Ypt11p, a rab-type small GTPase, is essential to facilitate the function of Myo2p, a class V myosin, in mitochondrial distribution in *Saccharomyces cerevisiae*. Mol. Cell. Biol. *22*, 7744–7757.

Izumi, T., Gomi, H., Kasai, K., Mizutani, S., and Torii, S. (2003). The roles of Rab27 and its effectors in the regulated secretory pathways. Cell Struct. Funct. *28*, 465–474.

Karcher, R. L., Deacon, S. W., and Gelfand, V. I. (2002). Motor-cargo interactions: the key to transport specificity. Trends Cell Biol. *12*, 21–27.

Kuroda, T. S., Fukuda, M., Ariga, H., and Mikoshiba, K. (2002). The Slp homology domain of synaptotagmin-like proteins 1–4 and Slac2 functions as a novel Rab27A binding domain. J. Biol. Chem. *277*, 9212–9218.

Langford, G. M. (2002). Myosin-V, a versatile motor for short-range vesicle transport. Traffic *3*, 859–865.

Luzio, J. P., Brake, B., Banting, G., Howell, K. E., Braghetta, P., and Stanley, K. K. (1990). Identification, sequencing and expression of an integral membrane protein of the trans-Golgi network (TGN38). Biochem. J. *270*, 97–102.

Matesic, L. E., Yip, R., Reuss, A. E., Swing, D. A., O'Sullivan, T. N., Fletcher, C. F., Copeland, N. G., and Jenkins, N. A. (2001). Mutations in Mlph, encoding a member of the Rab effector family, cause the melanosome transport defects observed in leaden mice. Proc. Natl. Acad. Sci. USA *98*, 10238–10243.

Mercer, J. A., Seperack, P. K., Strobel, M. C., Copeland, N. G., and Jenkins, N. A. (1991). Novel myosin heavy chain encoded by murine dilute coat colour locus. Nature *349*, 709–713.

Mermall, V., Post, P. L., and Mooseker, M. S. (1998). Unconventional myosins in cell movement, membrane traffic, and signal transduction. Science *279*, 527–533.

Miller, K. E., and Sheetz, M. P. (2000). Characterization of myosin V binding to brain vesicles. J. Biol. Chem. *275*, 2598–2606.

Molnar, E., Varadi, A., McIlhinney, R.A.J., and Ashcroft, S.J.H. (1995). Identification of functional ionotropic glutamate receptor proteins in pancreatic beta-cells and in islets of Langerhans. FEBS Lett. *371*, 253–257.

Nagashima, K., Torii, S., Yi, Z., Igarashi, M., Okamoto, K., Takeuchi, T., and Izumi, T. (2002). Melanophilin directly links Rab27a and myosin Va through its distinct coiled-coil regions. FEBS Lett. *517*, 233–238.

Nakata, T., and Hirokawa, N. (1992). Organization of cortical cytoskeleton of cultured chromaffin cells and involvement in secretion as revealed by quick-freeze, deep-etching, and double-label immunoelectron microscopy. J. Neurosci. *12*, 2186–2197.

Nascimento, A. A., Amaral, R. G., Bizario, J. C., Larson, R. E., and Espreafico, E. M. (1997). Subcellular localization of myosin-V in the B16 melanoma cells, a wild-type cell line for the dilute gene. Mol. Biol. Cell *10*, 1971–1988.

Pinton, P., Tsuboi, T., Ainscow, E. K., Pozzan, T., Rizzuto, R., and Rutter, G. A. (2002). Dynamics of glucose-induced recruitment of protein kinase C βII in living pancreatic islet β-cells. J. Biol. Chem. *277*, 37702–37710.

Pouli, A. E., Emmanouilidou, E., Zhao, C., Wasmeier, C., Hutton, J. C., and Rutter, G. A. (1998). Secretory granule dynamics visualised in vivo with a phogrin-green fluorescent protein chimaera. Biochem. J. *333*, 193–199.

Prekeris, R., and Terrian, D. M. (1997). Brain myosin V is a synaptic vesicle-associated motor protein: evidence for a Ca2+-dependent interaction with the synaptobrevin-synaptophysin complex. J. Cell Biol. *137*, 1589–1601.

Provance, D. W., Jr., Wei, M., Ipe, V., and Mercer, J. A. (1996). Cultured melanocytes from dilute mutant mice exhibit dendritic morphology and altered melanosome distribution. Proc. Natl. Acad. Sci. USA *93*, 14554–14558.

Provance, D. W., James, T. L., and Mercer, J. A. (2002). Melanophilin, the product of the leaden locus, is required for targeting of myosin-Va to melanosomes. Traffic *2*, 124–132.

Reck-Peterson, S. L., Provance, D. W., Jr., Mooseker, M. S., and Mercer, J. A. (2000). Class V myosins. Biochim. Biophys. Acta *1496*, 36–51.

Regazzi, R., Ravazzola, M., Lezzi, M., Lang, J. C., Zahraoui, A., Andereggen, E., Morel, P., Takai, Y., and Wollheim, C. B. (1996). Expression, localization and functional role of small GTPases of the Rab3 family in insulin-secreting cells. J. Cell Sci. *109*, 2265–2273.

Rudolf, R., Kogel, T., Kuznetsov, S. A., Salm, T., Schlicker, O., Hellwig, A., Hammer, J. A., 3rd, and Gerdes, H. H. (2003). Myosin Va facilitates the distribution of secretory granules in the F-actin rich cortex of PC12 cells. J. Cell Sci. *116*, 1339–1348.

Rutter, G. A. (2001). Nutrient-secretion coupling in the pancreatic islet β-cell: recent advances. Mol. Asp. Med. *22*, 247–284.

Rutter, G. A. (2004) Visualising Insulin Secretion. The Minkowski Lecture 2004. Diabetologia *47*, 1861–1872.

Schliwa, M. (1999). Molecular motors join forces. Nature *397*, 204–205.

Schott, D., Ho, J., Pruyne, D., and Bretscher, A. (1999). The COOH-terminal domain of Myo2p, a yeast myosin V, has a direct role in secretory vesicle targeting. J. Cell Biol. *147*, 791–808.

Seperack, P. K., Mercer, J. A., Strobel, M. C., Copeland, N. G., and Jenkins, N. A. (1995). Retroviral sequences located within an intron of the dilute gene alter dilute expression in a tissue-specific manner. EMBO J. *14*, 2326–2332.

Simon, V. R., Swayne, T. C., and Pon, L. A. (1995). Actin-dependent mitochondrial motility in mitotic yeast and cell-free systems: identification of a motor activity on the mitochondrial surface. J. Cell Biol. *130*, 345–354.

Strobel, M. C., Seperack, P. K., Copeland, N. G., and Jenkins, N. A. (1990). Molecular analysis of two mouse dilute locus deletion mutations: spontaneous dilute lethal20J and radiation-induced dilute prenatal lethal Aa2 alleles. Mol. Cell. Biol. *10*, 501–509.

Tabb, J. S., Molyneaux, B. J., Cohen, D. L., Kuznetsov, S. A., and Langford, G. M. (1998). Transport of ER vesicles on actin filaments in neurons by myosin V. J. Cell Sci. *111*, 3221–3234.

Takagishi, Y., Oda, S., Hayasaka, S., Dekker-Ohno, K., Shikata, T., Inouye, M., and Yamamura, H. (1996). The dilute-lethal (dl) gene attacks a Ca2+ store in the dendritic spine of Purkinje cells in mice. Neurosci. Lett. *215*, 169–172.

Torii, S., Takeuchi, T., Nagamatsu, S., and Izumi, T. (2004). Rab27 effector granuphilin promotes the plasma membrane targeting of insulin granules via interaction with syntaxin 1a. J. Biol. Chem. *279*, 22532–22538.

Torii, S., Zhao, S., Yi, Z., Takeuchi, T., and Izumi, T. (2002). Granuphilin modulates the exocytosis of secretory granules through interaction with syntaxin 1a. Mol. Cell. Biol. *22*, 5518–5526.

Tsuboi, T., Da Silva Xavier, G., Leclerc, I., and Rutter, G. A. (2003). 5′ AMP-activated protein kinase controls insulin-containing secretory vesicle dynamics. J. Biol. Chem. *278*, 52042–52051.

Tsuboi, T., and Rutter, G. A. (2003) Multiple forms of kiss and run exocytosis revealed by evanescent wave microscopy. Curr. Biol. *13*, 563–567.

Tsuboi, T., Zhao, C., Terakawa, S., and Rutter, G. A. (2000). Simultaneous evanescent wave imaging of insulin vesicle membrane and cargo during a single exocytotic event. Curr. Biol. *10*, 1307–1310.

Vallee, R. B., and Sheetz, M. P. (1996). Targeting of motor proteins. Science *271*, 1539–1544.

Varadi, A., Ainscow, E. K., Allan, V. J., and Rutter, G. A. (2002). Involvement of conventional kinesin in glucose-stimulated secretory-granule movements and exocytosis in clonal pancreatic β-cells. J. Cell Sci. *115*, 4177–4189.

Varadi, A., Molnar, E., Ostenson, C. G., and Ashcroft, S. J. (1996). Isoforms of endoplasmic reticulum Ca(2+)-ATPase are differentially expressed in normal and diabetic islets of Langerhans. Biochem. J. *319*, 521–527.

Varadi, A., Johnson-Cadwell, L. I., Cirulli, V., Yoon, Y., Allan, V. J., and Rutter, G. A. (2004). Cytoplasmic dynein regulates the subcellular distribution of mitochondria by controlling the recruitment of the fission factor dynamin-related protein-1. J. Cell Sci. *117*, 4389–4400.

Varadi, A., and Rutter, G. A. (2002). Dynamic imaging of endoplasmic reticulum $[Ca^{2+}]$ in MIN6 β-cells using recombinant chameleons: roles of SERCA2 and ryanodine receptors. Diabetes *51*, S190–S201.

Varadi, A., Tsuboi, T., Johnson-Cadwell, L. I., Allan, V. J., and Rutter, G. A. (2003). Kinesin I and cytoplasmic dynein orchestrate glucose-stimulated insulin-containing vesicle movements in clonal MIN6 beta-cells. Biochem. Biophys. Res. Commun. *311*, 272–282.

Verhey, K. J., Meyer, D., Deehan, R., Blenis, J., Schnapp, B. J., Rapoport, T. A., and Margolis, B. (2001). Cargo of kinesin identified as JIP scaffolding proteins and associated signaling molecules. J. Cell Biol. *152*, 959–970.

Wang, J., Takeuchi, T., Yokota, H., and Izumi, T. (1999). Novel rabphilin-3-like protein associates with insulin-containing granules in pancreatic beta cells. J. Biol. Chem. *274*, 28542–28548.

Waselle, L., Coppola, T., Fukuda, M., Iezzi, M., El Amraoui, A., Petit, C., and Regazzi, R. (2003). Involvement of the Rab27 binding protein Slac2c/MyRIP in insulin exocytosis. Mol. Biol. Cell *14*, 4103–4113.

Wasmeier, C., and Hutton, J. C. (1996). Molecular cloning of phogrin, a protein-tyrosine phosphatase homologue localized to insulin secretory granule membranes. J. Biol. Chem. *271*, 18161–18170.

Weber, K. L., Sokac, A. M., Berg, J. S., Cheney, R. E., and Bement, W. M. (2004). A microtubule-binding myosin required for nuclear anchoring and spindle assembly. Nature *431*, 325–329.

Wu, X., Bowers, B., Rao, K., Wei, Q., and Hammer, J. A. (1998). Visualization of melanosome dynamics within wild-type and dilute melanocytes suggests a paradigm for myosin V function in vivo. J. Cell Biol. *143*, 1899–1918.

Wu, X. S., Rao, K., Zhang, H., Wang, F., Sellers, J. R., Matesic, L. E., Copeland, N. G., Jenkins, N. A., and Hammer, J. A., 3rd. (2002a) Identification of an organelle receptor for myosin-Va. Nat. Cell Biol. *4*, 271–278.

Wu, X., Wang, F., Rao, K., Sellers, J. R., and Hammer, J. A., 3rd. (2002b) Rab27a is an essential component of melanosome receptor for myosin Va. Mol. Biol. Cell *5*, 1735–1749.

Yaekura, K., *et al*. (2003). Insulin secretory deficiency and glucose intolerance in Rab3A null mice. J. Biol. Chem. *278*, 9715–9721.

Yi, M., Weaver, D., and Hajnoczky, G. (2004). Control of mitochondrial motility and distribution by the calcium signal: a homeostatic circuit. J. Cell Biol. *167*, 661–672.

Yi, Z., Yokota, H., Torii, S., Aoki, T., Hosaka, M., Zhao, S., Takata, K., Takeuchi, T., and Izumi, T. (2002). The Rab27a/granuphilin complex regulates the exocytosis of insulin-containing dense-core granules. Mol. Cell. Biol. *22*, 1858–1867.